Design methodology and performance analysis of a wideband 90° phase switch for radiometer applications

Enrique Villa,[a] Beatriz Aja, Jaime Cagigas, Luisa de la Fuente, and Eduardo Artal
Department of Communications Engineering, University of Cantabria, Plaza de la Ciencia s/n, Santander 39005, Spain

(Received 4 September 2013; accepted 3 December 2013; published online 27 December 2013)

This paper presents the analysis, design, and characterization of a wideband 90° phase switch in Ka-band. The phase switch is based on two microstrip bandpass filters in which the commutation is performed by a novel single-pole double-throw (SPDT) switch. The analysis of π-network bandpass filters is provided, obtaining the phase difference and amplitude imbalance between filters and their scattering parameters; tested results show an average phase difference of 88.9° ± 5° and an amplitude imbalance of 0.15 dB from 24 to 37 GHz. The new broadband SPDT switch is based on a coplanar waveguide-to-slotline-to-microstrip structure, which enables a full planar integration with shifting branches. PIN diodes are used to perform the switching between outputs. The SPDT shows isolation better than 19 dB, insertion loss of around 1.8 dB, and return loss better than 15 dB. The full integration of the phase switch achieves a return loss better than 11 dB and insertion loss of around 4 dB over the band 26–36 GHz, with an average phase difference of 87.1° ± 4° and an average amplitude imbalance of 0.3 dB. It provides an excellent performance for this frequency range, suitable for radio-astronomy receivers. © *2013 AIP Publishing LLC*. [http://dx.doi.org/10.1063/1.4849555]

I. INTRODUCTION

Phase switches are two-port networks providing a fixed phase difference with low-amplitude imbalance between two states in a defined bandwidth.[1] As an initial design approach, a phase switch is based on a phase shifter, which is a four-port passive network, introducing a constant phase difference. The four-port device is turned into a two-port one by using two in-phase three-port microwave switching circuits, in which DC signals modulate the circuit behavior. Phase switches are relevant components in several wideband applications, such as phased-array antennas, phase modulators, control applications, or as a part of microwave measurement systems.

The design of wideband phase shifters has been widely described in the literature using quite different topologies.[1–17] Since Schiffman[1] designed λ/4 coupled-line sections achieving 90° phase shift in an octave bandwidth, many approaches based on transmission lines,[2–9] bandpass filters related to a reference transmission line,[10–15] or reflection-type,[16] have been implemented to improve the operating bandwidth or phase imbalance. Most phase shifter arrangements are designed using a transmission line as a reference circuit. Other approaches use modified configurations instead of the transmission line, synthesizing coupled section,[7] or bandpass filter (BPF) topologies[11,13,17] as reference circuits.

Phase switches are essential components in many applications, such as phased-array antennas, modulators, microwave systems, or receivers. Some of these receivers with phase switches are used in radio-astronomy, typically in radiometers[18–20] and interferometers.[21] These radiometers are high-sensitivity coherent direct detection receivers designed for sky observation, in which the phase switching ensures that gain fluctuations in the low-noise amplification chain do not affect the overall radiometer stability. The receivers for the PLANCK,[18] QUIET,[19] and FARADAY[20] experiments were developed using 180° phase switches to characterize the cosmic microwave background (CMB), which is the most important source of information about the evolution of the universe. A recent experiment, the QUIJOTE project,[22,23] is developing a ground-based receiver in order to characterize the polarization of the CMB and other galactic emissions. The radiometer will be able to simultaneously measure three of the Stokes parameters (Q, U, and I), which describe the polarization state of an electromagnetic wave. The receiver scheme comprises 0/180° and 0/90° phase switches to generate four polarization states and their performance is crucial in order to obtain the Stokes parameters,[23] minimizing leakage among them and, at the same time, overcoming the 1/f noise and different systematic errors in the receiver.

This paper presents the analysis, design, and characterization of a 90° phase switch based on BPF combination as shifting branches. The design is focused on covering the frequency band from 26 to 36 GHz, with the aim of being used in QUIJOTE Phase II receivers. The BPFs are analyzed in order to obtain the phase behavior between branches. Full analysis is provided in order to make tradeoffs between phase and insertion-return loss of the branches. Moreover, the full phase switch performance is analyzed in terms of phase difference and amplitude imbalance errors due to SPDT mismatching and isolation. The designs of the BPFs and a novel SPDT switch using planar technology are also described. The SPDT combines coplanar waveguide (CPW), slotline, and microstrip technologies. After the description of the phase switch analysis in Sec. II, the designs of the BPFs and the SPDT based on modified CPW-to-slotline transitions which

[a]Author to whom correspondence should be addressed. Electronic mail: villae@unican.es

make up the phase switch are discussed in Sec. III. The fabrication and characterization of individual filters, the SPDT and fully integrated phase switch, as well as a comparison with other previous reported works are described in Sec. IV. Finally, Sec. V draws general conclusions.

II. PHASE SWITCH ANALYSIS

The proposed topology for the 90° phase switch is shown in Fig. 1, consisting of two BPF branches and two SPDT switches. The BPFs are suitable for a radio-astronomy receiver, since they enable an operating frequency band to be defined and the effective bandwidth of the radiometer to be sustained in both states of the phase switch. Therefore, the design is focused on achieving a flat 90° phase shift over a broad frequency range, as well as a low amplitude imbalance between branches and low return loss.

In Secs. II A–II C, the phase switch analysis is discussed. The BPF branches are considered as π-networks, in which the phase shift of the circuit is the difference between each individual BPF phase at the center frequency f_0 as expressed in Eq. (1):

$$\Delta\Phi(f_0) = \Phi_{\mathrm{BPF\#1}}(f_0) - \Phi_{\mathrm{BPF\#2}}(f_0). \tag{1}$$

The expression of the phase difference over a frequency range is obtained. The return and insertion loss are discussed in order to consider them as design goals.

A. π-network BPF admittance matrix

The BPFs considered in the design are based on symmetrical π-topologies using shunt open-circuited stubs. The basic π-network topology which is analyzed is shown in Fig. 2(a). The equivalent admittance matrix, depicted in Fig. 2(b), of a single π-network can be easily derived from circuit analysis.

The Y-matrix of open-circuited stub π-networks at f_0 is given by (2):

$$[Y] = j \cdot \begin{bmatrix} Y_P \cdot \tan(\theta_{si}) - Y_S \cdot \cot(\theta_i) & Y_S \cdot \csc(\theta_i) \\ Y_S \cdot \csc(\theta_i) & Y_P \cdot \tan(\theta_{si}) - Y_S \cdot \cot(\theta_i) \end{bmatrix}, \tag{2}$$

where $Y_P = 1/Z_P$ and $Y_S = 1/Z_S$ are the admittances of the transmission lines and θ_i are their electrical lengths.

Since the analyzed π-network is symmetrical, using Eq. (2), the transmission phase can be expressed at f_0 as

$$\begin{aligned}\Phi_\pi(f_0) &= \cos^{-1}\left(-\frac{Y_{11}}{Y_{12}}\right) \\ &= \cos^{-1}\left(\frac{-Y_P \cdot \tan(\theta_{si}) + Y_S \cdot \cot(\theta_i)}{Y_s \cdot \csc(\theta_i)}\right).\end{aligned} \tag{3}$$

It is observed that Eq. (3) can be solved only when the following condition is satisfied:

$$|Y_{11}| \le |Y_{12}|. \tag{4}$$

When $Z_P = Z_S$, Eq. (3) can be rewritten as

$$\Phi_\pi(f_0) = \cos^{-1}\left(\frac{\cos(\theta_{si} + \theta_i)}{\cos(\theta_{si})}\right). \tag{5}$$

B. Phase difference performance

The 90° phase switch is based on two BPFs designed using π-networks. The topology of BPF #1 in Fig. 1 is composed of a π-network with a pair of series transmission lines in its accesses. On the other hand, BPF #2 in Fig. 1 uses two cascaded π-networks. Both BPF schematics are depicted in Fig. 3.

Substituting the impedances and electrical lengths of each BPF in Fig. 3 into Eq. (2), the Y-parameters of the branches can be obtained, and applying Eq. (3), the transmission phases of each BPF at an arbitrary frequency are

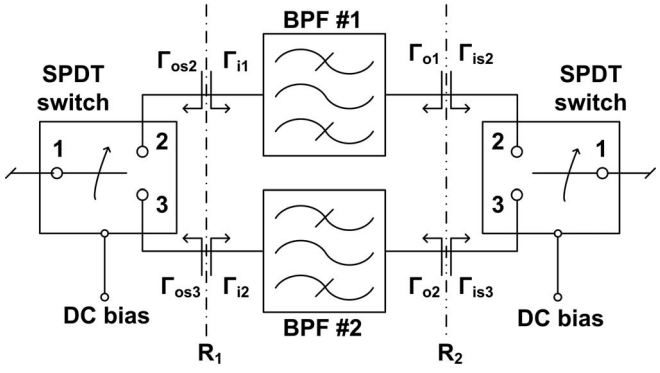

FIG. 1. Proposed topology for the 90° phase switch.

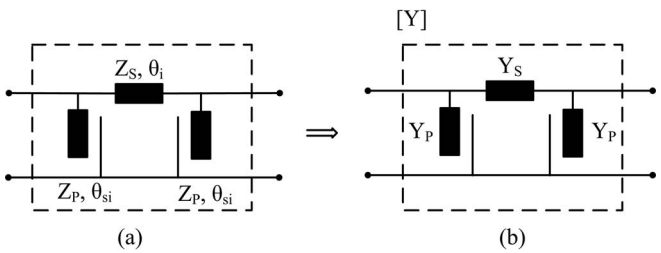

FIG. 2. π-network topology. (a) Single network. (b) Equivalent Y-matrix.

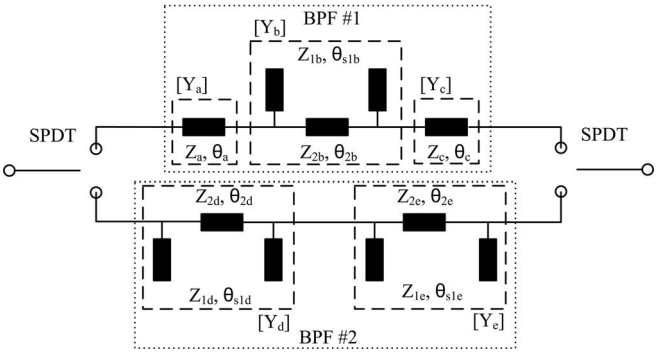

FIG. 3. BPF schematics of the proposed 90° phase switch.

given by

$$\Phi_{\mathrm{BPF\,\#1}}(\eta)=\cos^{-1}\left(\frac{-Y_{1b}\cdot\tan(\eta\cdot\theta_{s1b})+Y_{2b}\cdot\cot(\eta\cdot\theta_{2b})}{Y_{2b}\cdot\csc(\eta\cdot\theta_{2b})}\right)+\eta\cdot(\theta_a+\theta_c), \tag{6}$$

$$\Phi_{\mathrm{BPF\,\#2}}(\eta)=\cos^{-1}\left(\frac{-Y_{1d}\cdot\tan(\eta\cdot\theta_{s1d})+Y_{2d}\cdot\cot(\eta\cdot\theta_{2d})}{Y_{2d}\cdot\csc(\eta\cdot\theta_{2d})}\right)+\cos^{-1}\left(\frac{-Y_{1e}\cdot\tan(\eta\cdot\theta_{s1e})+Y_{2e}\cdot\cot(\eta\cdot\theta_{2e})}{Y_{2e}\cdot\csc(\eta\cdot\theta_{2e})}\right), \tag{7}$$

where $\eta = f/f_0$ is the normalized frequency, $Y_i = 1/Z_i$ is the admittance, and θ_i is the electrical length of each transmission line.

Finally, to obtain the phase difference of the phase switch, Eqs. (6) and (7) are substituted into Eq. (1).

In the analysis that follows, both BPFs consist of quarter-wavelength in series transmission lines and half-wavelength in shunt ones at the center frequency f_0 and the π-networks in BPF #2 are identical ($Z_{1d} = Z_{1e}$ and $Z_{2d} = Z_{2e}$). The impedances of the input Z_a and output Z_c transmission lines in BPF #1 are assumed to be the same values as the series impedance of the π-network in its branch Z_{2b}.

Hence, the phase difference between branches is expressed as

$$\Delta\Phi(\eta) = \eta\cdot\pi+\cos^{-1}\left(\frac{-Y_{1b}}{Y_{2b}}\cdot\tan(\eta\pi)\cdot\sin\left(\eta\frac{\pi}{2}\right)+\cos\left(\eta\frac{\pi}{2}\right)\right) -2\cdot\cos^{-1}\left(\frac{-Y_{1d}}{Y_{2d}}\cdot\tan(\eta\pi)\cdot\sin\left(\eta\frac{\pi}{2}\right)+\cos\left(\eta\frac{\pi}{2}\right)\right). \tag{8}$$

The phase difference expression shows the dependence on the admittances of the transmission lines. A range of admittance ratios between $1/\sqrt{2}$ and 2 are considered for Y_{1b}/Y_{2b} and Y_{1d}/Y_{2d}, and a combination of these values is taken in Eq. (8). The phase error *PE* is analyzed in the band of interest (26–36 GHz, center frequency $f_0 = 31$ GHz) and it is defined as

$$PE(^\circ) = |90^\circ - |\Delta\Phi(^\circ)||. \tag{9}$$

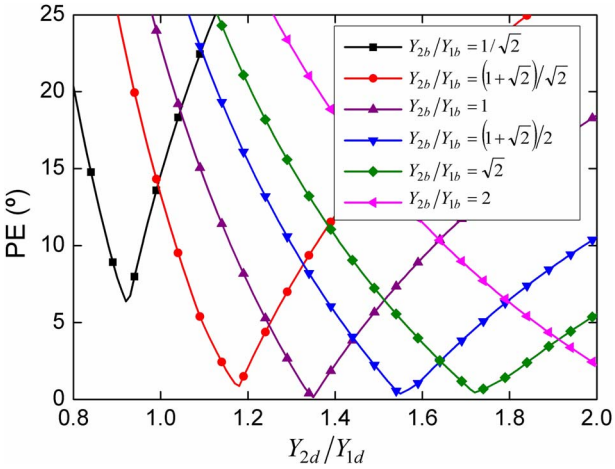

FIG. 4. Maximum phase error versus admittance ratios of BPF #1 in the frequency band from 26 to 36 GHz for different admittance ratios of BPF #2.

The maximum value of the phase error over the frequency band 26–36 GHz, for a combination of admittances for BPF #1 and BPF #2, is shown in Fig. 4. Considering a *PE* lower than 0.5°, three minimum in-band values are obtained when the ratios (Y_{2b}/Y_{1b}, Y_{2d}/Y_{1d}) are set to [(1, 1.35), ($(1+\sqrt{2})/2$, 1.55), ($\sqrt{2}$, 1.72)].

On the other hand, the S-parameters of the BPFs are calculated, analyzing their amplitude imbalance (*AI*) and return loss. *AI* is defined as

$$AI(\mathrm{dB}) = 10\cdot\log 10|S_{21\mathrm{BPF\,\#1}}/S_{21\mathrm{BPF\,\#2}}|^2. \tag{10}$$

A minimum value, over the band 26–36 GHz, in Eq. (10) is desired and, simultaneously, optimum return loss. Assuming the ratios of admittances (Y_{2b}/Y_{1b}, Y_{2d}/Y_{1d}) in each branch for minimum *PE*, the admittances Y_{2b} and Y_{2d} are swept in a range between $1/\sqrt{2}\cdot Y_0$ and $\sqrt{2}/Y_0$ ($Y_0 = 1/50$) and the *AI* are analyzed. The maximum value of the amplitude imbalance for each sweep is calculated in the 26–36 GHz frequency range. The sweeps which provide the smallest value of *AI* are shown in Fig. 5 versus $1/\overline{Y_{2d}}$, since the $1/\overline{Y_{2b}}$ sweep provides an optimum value equal to 1. An optimum value for *AI* is achieved when the normalized admittances for both

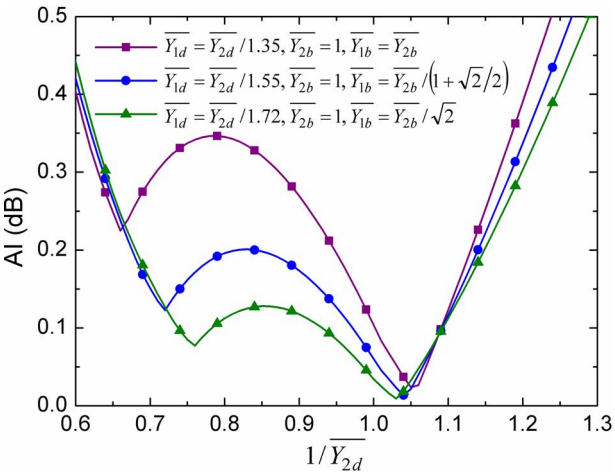

FIG. 5. Maximum amplitude imbalance versus normalized series admittance, $\overline{Y_{2d}}$, in the frequency band from 26 to 36 GHz for different admittance ratios.

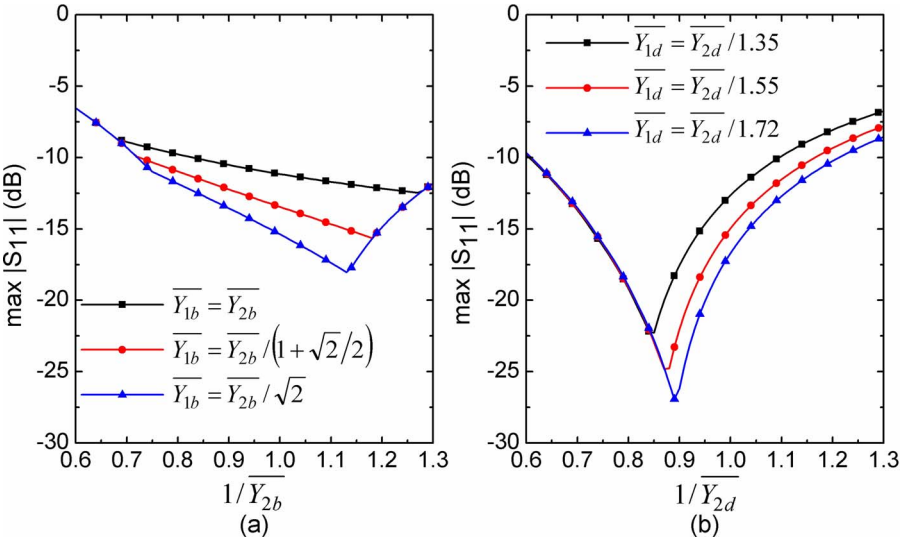

FIG. 6. Maximum input return loss versus normalized series admittances in the frequency band from 26 to 36 GHz. (a) BPF #1. (b) BPF #2.

filters are equal to $1/\overline{Y_{2d}} = 1.03$, $\overline{Y_{1d}} = \overline{Y_{2d}}/1.72$, $\overline{Y_{2b}} = 1$, and $\overline{Y_{1b}} = \overline{Y_{2b}}/\sqrt{2}$.

Moreover, the return loss in each branch is analyzed for the same sweeps. The maximum return loss over the frequency range from 26 to 36 GHz versus normalized series admittance is depicted in Fig. 6 for both filters. The optimum values are achieved when $1/\overline{Y_{2b}} = 1.13$ for BPF #1 and $1/\overline{Y_{2d}} = 0.89$ for BPF #2. When the lowest *AI* value is considered, the maximum return loss is better than 15 dB for both filters.

The above analysis shows optimum *AI* and return loss for different values of the swept normalized series admittance, but close to 1. Therefore, as a tradeoff between *AI* and return loss, the normalized series admittances $\overline{Y_{2d}}$ and $\overline{Y_{2b}}$ are fixed to 1 as initial approach and the admittance ratios of $(Y_{2b}/Y_{1b}, Y_{2d}/Y_{1d}) = (\sqrt{2}, 1.72)$ are selected.

The phase difference for the admittance ratio $(Y_{2b}/Y_{1b}, Y_{2d}/Y_{1d}) = (\sqrt{2}, 1.72)$ is given by

$$\begin{aligned}\Delta\Phi(\eta) &= \eta\cdot\pi + \cos^{-1}\left(\frac{-1}{\sqrt{2}}\cdot\tan(\eta\pi)\cdot\sin\left(\eta\frac{\pi}{2}\right)+\cos\left(\eta\frac{\pi}{2}\right)\right)\\ &\quad -2\cdot\cos^{-1}\left(\frac{-1}{1.72}\cdot\tan(\eta\pi)\cdot\sin\left(\eta\frac{\pi}{2}\right)+\cos\left(\eta\frac{\pi}{2}\right)\right).\end{aligned} \tag{11}$$

The input return loss and insertion loss of each BPF are calculated using the cascaded admittance matrixes of each subnetwork and series transmission lines (Z_a and Z_c), which are given by

$$[Y_a] = [Y_c] = j\cdot\begin{bmatrix}\frac{1}{50}\cdot\cot\left(\eta\frac{\pi}{2}\right) & \frac{1}{50}\cdot\csc\left(\eta\frac{\pi}{2}\right)\\ \frac{1}{50}\cdot\csc\left(\eta\frac{\pi}{2}\right) & \frac{1}{50}\cdot\cot\left(\eta\frac{\pi}{2}\right)\end{bmatrix}, \tag{12}$$

$$[Y_b] = j\cdot\begin{bmatrix}\frac{1}{70.7}\cdot\tan(\eta\pi)-\frac{1}{50}\cdot\cot\left(\eta\frac{\pi}{2}\right) & \frac{1}{50}\cdot\csc\left(\eta\frac{\pi}{2}\right)\\ \frac{1}{50}\cdot\csc\left(\eta\frac{\pi}{2}\right) & \frac{1}{70.7}\cdot\tan(\eta\pi)-\frac{1}{50}\cdot\cot\left(\eta\frac{\pi}{2}\right)\end{bmatrix}, \tag{13}$$

$$[Y_d] = [Y_e] = j\cdot\begin{bmatrix}\frac{1}{86}\cdot\tan(\eta\pi)-\frac{1}{50}\cdot\cot\left(\eta\frac{\pi}{2}\right) & \frac{1}{50}\cdot\csc\left(\eta\frac{\pi}{2}\right)\\ \frac{1}{50}\cdot\csc\left(\eta\frac{\pi}{2}\right) & \frac{1}{86}\cdot\tan(\eta\pi)-\frac{1}{50}\cdot\cot\left(\eta\frac{\pi}{2}\right)\end{bmatrix}. \tag{14}$$

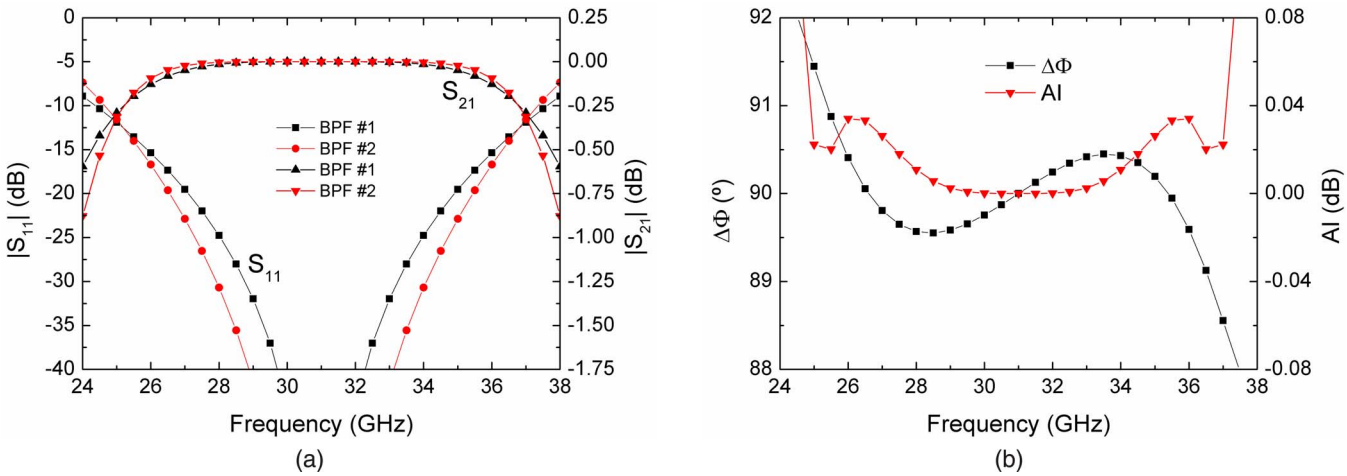

FIG. 7. Ideal response of BPFs. (a) Return loss and insertion loss. (b) Phase difference and amplitude imbalance.

The performances in terms of input return loss, insertion loss, phase difference, and amplitude imbalance from 24 to 38 GHz of the ideal BPFs are depicted in Fig. 7. As a conclusion, using the proposed 90° phase shifter enables minimum phase error and amplitude imbalance to be achieved, as well as remarkable return loss in the band of interest. The circuit analysis shows that a design using quarter- and half-wavelength for series and shunt transmission lines, respectively, at the center frequency f_0, with a ratio of admittances defined by $(Y_{2b}/Y_{1b}, Y_{2d}/Y_{1d}) = (\sqrt{2}, 1.72)$ considering $Y_{1b} = Y_{1d} = 1/Z_0$ satisfies the requirements of phase error, amplitude imbalance, and matching.

C. SPDT non-idealities impact

The phase switch is considered as the block diagram shown in Fig. 1, in which the reflection coefficients between subnetworks are described. These coefficients enable the mismatching effects (reference planes R_1 and R_2) to be analyzed in terms of error in phase difference ($E\Phi$) and amplitude imbalance (EAI). Besides, the effect of the isolated branch is also considered.

The analysis considers reciprocal and identical SPDTs and is fulfilled when the transmission is performed by BPF #1. The analysis for the switched state transmitting by BPF #2 ($S_{21\mathrm{BPF\,\#2\_}C}$) is analogous. The S-matrix of the whole circuit is obtained, defining SPDTs and BPFs by their S-matrixes composed of terms S_{ijS} (i, j = 1, 2, 3) for the SPDT and $S_{ij\mathrm{BPF\,\#}k}$ (i, j = 1, 2) for the BPFs and k = 1, 2 indicates the filter. The transmission parameter in this state is given by

$$S_{21\mathrm{BPF\#1\_C}} = \frac{1}{1 - F - B + B \cdot F - C \cdot E} \cdot \left[\frac{S_{21S} \cdot S_{21\mathrm{BPF\#1}} \cdot (D + E \cdot A - B \cdot D)}{(1 - S_{22\mathrm{BPF\#1}} \cdot \Gamma_{is2})} + \frac{S_{31S} \cdot S_{21\mathrm{BPF\#2}} \cdot (D + E \cdot A - B \cdot D)}{(1 - S_{22\mathrm{BPF\#2}} \cdot S_{33S})} \right], \quad (15)$$

where

$$\Gamma_{is2} = S_{22S} + \frac{S_{32S}^2 \cdot \Gamma_{o2}}{1 - S_{33S} \cdot \Gamma_{o2}}, \quad (16)$$

$$\Gamma_{o2} = S_{22\mathrm{BPF\#2}} + \frac{S_{21\mathrm{BPF\#2}}^2 \cdot S_{33S}}{1 - S_{11\mathrm{BPF\#1}} \cdot S_{33S}}, \quad (17)$$

$$\Gamma_{i1} = S_{11\mathrm{BPF\#1}} + \frac{S_{21\mathrm{BPF\#1}}^2 \cdot \Gamma_{is2}}{1 - S_{22\mathrm{BPF\#1}} \cdot \Gamma_{is2}}, \quad (18)$$

$$\Gamma_{i2} = S_{11\mathrm{BPF\#2}} + \frac{S_{21\mathrm{BPF\#2}}^2 \cdot S_{33S}}{1 - S_{22\mathrm{BPF\#2}} \cdot S_{33S}}, \quad (19)$$

and $A = S_{21S}$, $B = S_{22S} \cdot \Gamma_{i1}$, $C = S_{32S} \cdot \Gamma_{i2}$, $D = S_{31S}$, $E = S_{32S} \cdot \Gamma_{i1}$, and $F = S_{33S} \cdot \Gamma_{i2}$.

Both transmission parameters for each circuit state are obtained, which enable the errors in phase difference and amplitude imbalance to be calculated by subtracting the calculated phase difference and amplitude imbalance of the phase switch to the values of the ideal BPFs (AI and $\Delta\Phi$), shown in Fig. 7. These errors are defined by

$$\mathrm{EAI} = 10 \cdot \log 10 |S_{21\mathrm{BPF\#1\_C}} / S_{21\mathrm{BPF\#2\_C}}|^2 - AI, \quad (20)$$

$$E\Phi = \angle(S_{21\mathrm{BPF\#1\_C}} / S_{21\mathrm{BPF\#2\_C}}) - \Delta\Phi. \quad (21)$$

The above expressions take into account the non-idealities of each subsystem and the interaction between them. SPDTs isolation (S_{31S}) and output return loss (S_{22S}) are swept over the operating frequency range. High isolation between output ports of the SPDTs is considered, so its impact is negligible. Figures 8(a) and 8(b) depict the errors in phase and amplitude for different isolation values and perfect matching at transmitting output. Isolation greater than 16 dB provides phase errors and amplitude errors lower than 5° and 0.6 dB in the band from 26 to 36 GHz. In Figs. 8(c) and 8(d), a 16 dB isolation is considered and the SPDTs output return loss are swept. Therefore, mismatching errors in SPDT interconnections are analyzed. When output return loss is better than

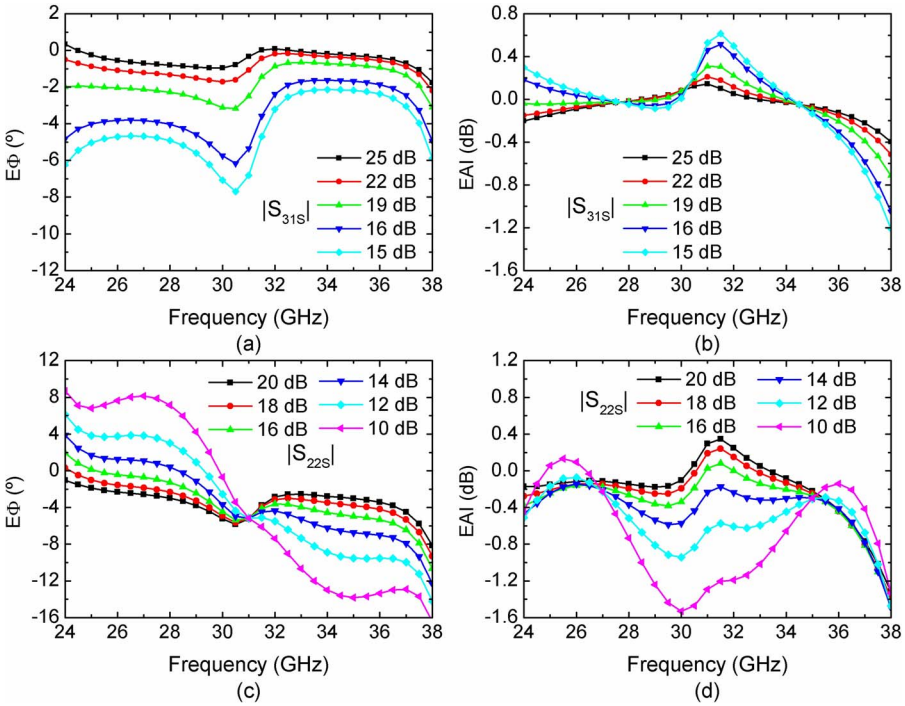

FIG. 8. Errors in phase ($E\Phi$) and amplitude imbalance (EAI) of the phase switch relative to ideal $\Delta\Phi$ and AI of the BPFs. (a) and (b) SPDT isolation sweep with perfect output return loss; (c) and (d) SPDT output return loss sweep with isolation $|S_{31S}| = 16$ dB.

14 dB, phase errors and amplitude errors lower than 6° and 0.6 dB in the band from 26 to 36 GHz are obtained.

As a conclusion, the impact of the SPDTs behavior in the full phase switch performance is analyzed and becomes significant in phase difference and amplitude imbalance deviation when isolation and output return loss are worse than 16 dB and 14 dB, respectively.

III. PHASE SWITCH DESIGN

To verify the proposed topology for the phase switch and the theoretical approach developed in Sec. II, a prototype of the phase switch is designed. The analysis in Sec. II B determines initial design parameters of the BPFs that provide the phase difference. In order to have a phase switch with the complete functionality, a SPDT that commutates between filters is also developed, taking into account the requirements of isolation and return loss described in Sec. II C.

A. Bandpass filter design

The BPF designs are aided with electromagnetic simulators using microstrip technology. The filters are designed on a 0.254-mm alumina substrate ($\varepsilon_r = 9.9$, $\tan\delta = 0.0001$).

Initial parameters for the transmission lines are set as was determined in theoretical analysis for the impedance and electrical length values. Since a microstrip approach is considered, interconnections (T-junctions) between transmission lines are taken into account due to their relevant effect in millimeter-wave frequencies. Therefore, design parameters are optimized in order to fulfill *PE*, *AI*, and return loss requirements.

As can be observed in Fig. 3, the BPF #2 is divided into two cascaded π-networks. Thus, the shunt stubs of each network, connected to the same electrical point and with the same impedances ($Z_{1d} = Z_{1e}$), are simplified to an equivalent shunt stub with the same impedance value and an equivalent electrical length given by

$$\theta_{seq} = \cot^{-1}\left(\cot\left(\theta_{s1d}\right) + \cot\left(\theta_{s1e}\right)\right). \tag{22}$$

The schematic of both BPFs with the equivalent shunt stub in BPF #2 is depicted in Fig. 9. Moreover, it shows the dimensions of the different transmission lines, in terms of widths and physical lengths after optimization process.

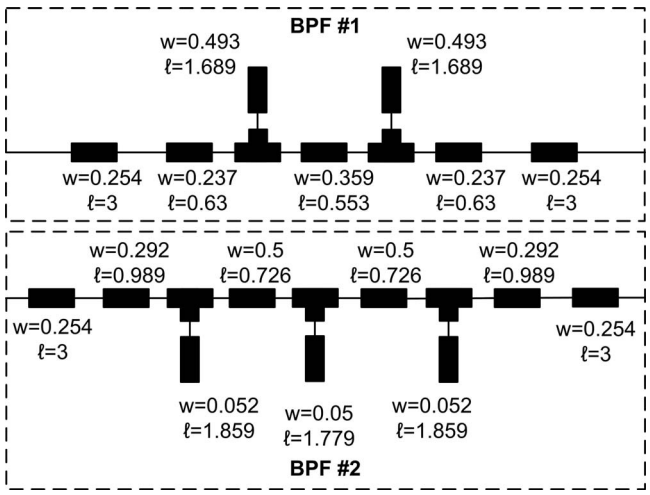

FIG. 9. BPF schematics with dimensions of the microstrip lines (dimensions in mm).

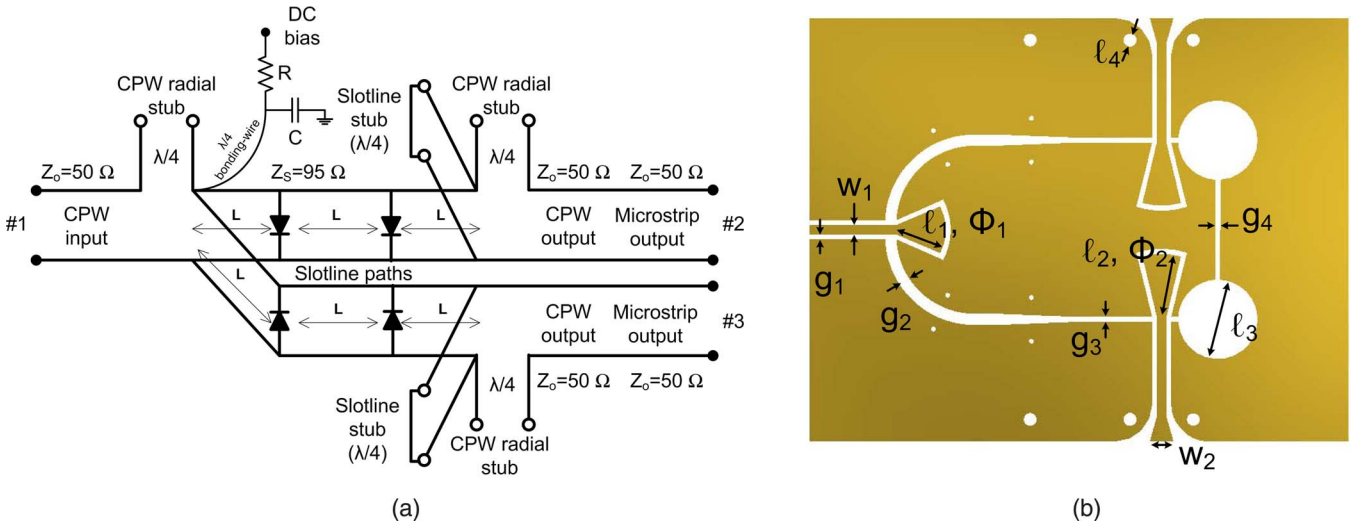

FIG. 10. CPW-slotline-microstrip SPDT. (a) Schematic diagram of the (L = λ/4 at center frequency). (b) Layout showing circuit dimensions.

B. Novel SPDT design

The commutation between BPFs is performed by a SPDT switch. Since this circuit selects the propagation branch of the phase switch, the isolation between SPDT arms is significant. High isolation values ensure negligible leakage signal from the switched-out branch and avoid degradation of the phase switch performance. Moreover, the aim of the SPDT is to provide low return loss level and flat insertion loss over the operating bandwidth.

A novel circuit is designed in CPW, slotline, and microstrip technologies, in the same substrate as the BPFs. This solution enables an easy integration of the SPDT with the phase shifting branches, making possible to develop the entire phase switch in planar technology. Furthermore, this solution avoids the use of bond wire interconnections to an external SPDT, such as a monolithic microwave integrated circuit, which affects the whole circuit behavior due to their direct impact on phase at these frequencies.

A simplified schematic of the SPDT is shown in Fig. 10(a). It is based on the use of a modified CPW to slotline transition: it has double and symmetric output ways in which the short-circuited quarter-wavelength slotline stub is performed by a diode. The use of slotlines facilitates the assembly of switching devices. In order to improve isolation results, two switching elements are used in each slotline branch, so the equivalent electrical length of each slotline way is three quarter-wavelength. The devices are placed at a quarter-wavelength electrical distance from the input and output CPW-to-slotline transitions and between them. Besides, a transition from CPW to microstrip line is implemented in order to connect the BPFs with the SPDT. The layout of the SPDT is shown in Fig. 10(b), in which the dimensions of the CPW and slotlines are defined and they are listed in Table I. The CPW and slotline circuits are designed with no bottom metallization, whereas for the microstrip it is provided. Therefore, the etching of back metallization is added in the CPW-to-microstrip transition, implementing 0.2 mm radius via holes to improve the response. The side CPW contacts are gradually tapered. In order to bias the switching devices, a narrow gap is introduced between slotline round stubs. This gap creates an isolated area where a DC bias point could be provided.

IV. CHARACTERIZATION

S-parameter tests of the BPFs, the SPDT, and the full integrated phase switch are performed in the Ka-band. The characterization is done using a coplanar probe station and a vector network analyzer (E8364A from Agilent Technologies).

A. Bandpass filter characterization

Both BPFs are tested in order to validate their performance. Measured results are shown in Fig. 11, in which they are compared to the electromagnetic simulations.

The measured results are consistent with the electromagnetic simulations, obtaining input return loss better than 13 dB and insertion loss of about 0.5 dB. Phase difference result shows an average value of 88.9° ± 5° and an average amplitude imbalance of 0.15 dB from 24 to 37 GHz. Therefore, a relative bandwidth of 42 % is achieved. Considering the bandwidth of the radiometer (from 26 to 36 GHz), a phase difference of 88.8° ± 1.1° is obtained.

TABLE I. Physical dimensions of the SPDT.

Variable	Value (mm)	Variable	Value
g_1, g_3, g_4	0.05	ℓ_2	0.66 mm
g_2	0.121	ℓ_3	0.85 mm
w_1	0.104	ℓ_4	0.2 mm
w_2	0.25	Φ_1	45°
ℓ_1	0.51	Φ_2	27°

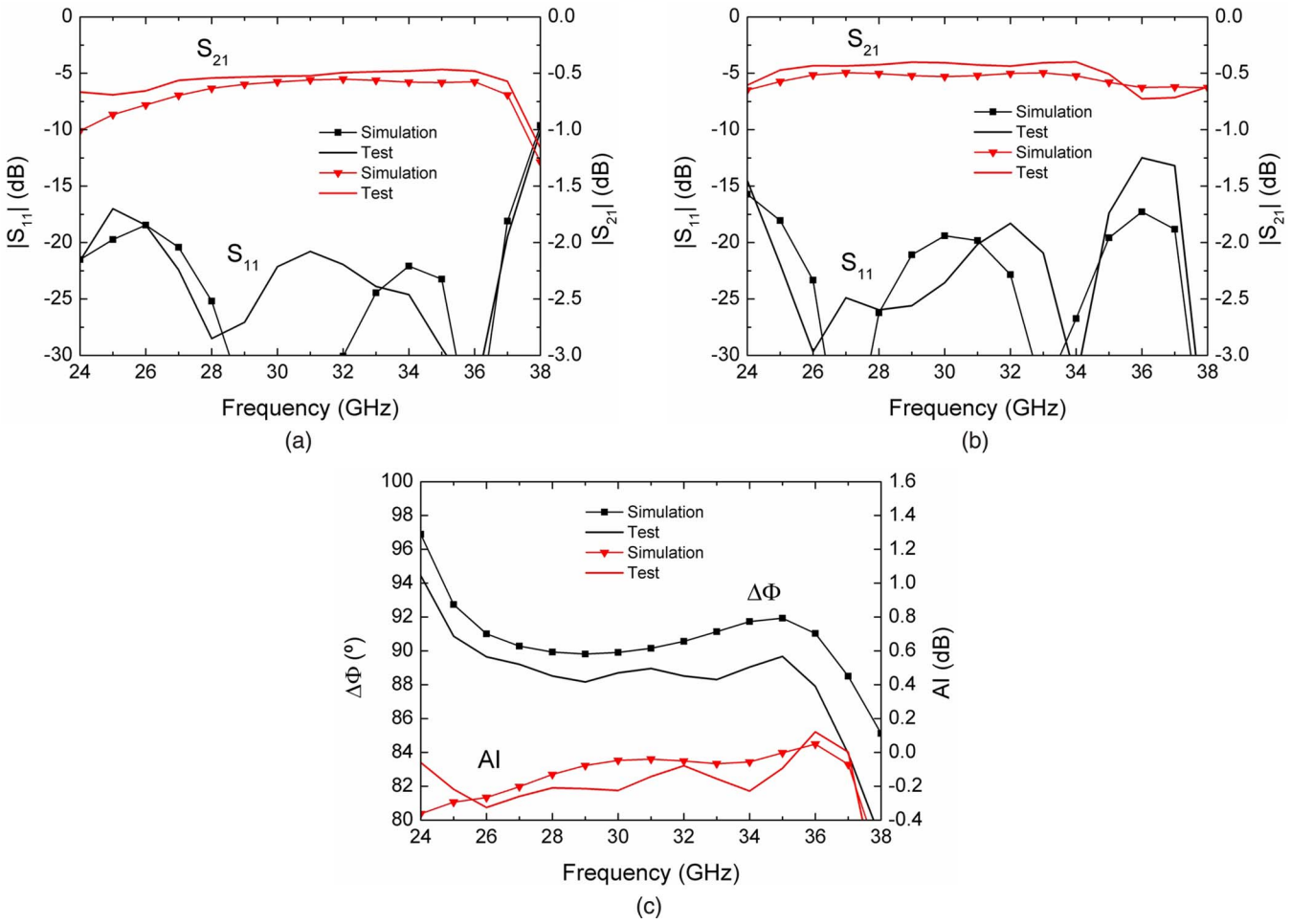

FIG. 11. Microstrip BPF tests and electromagnetic simulations comparison. (a) BPF #1 S-parameters. (b) BPF #2 S-parameters. (c) Phase difference and amplitude imbalance between BPFs.

B. SPDT characterization

A photograph of the SPDT is shown in Fig. 12. The SPDT is individually measured without microstrip transitions for measurement feasibility reasons. In order to validate the performance of the circuit, the switching devices must show an equivalent low series resistance in its ON state, whereas a low capacitance in its OFF state. The selected devices are microwave PIN diodes model HPND-4005 from Avago Technologies. The SPDT performance in one of its state is shown in Fig. 13, defining the reference planes at the CPW accesses. The measurements show remarkable isolation, better than 19 dB (S_{31S}) in the frequency band from 26 GHz to 36 GHz, with low insertion loss of 1.8 dB, return loss level in accesses better than 15 Db, and transmission loss from coupled to isolated ports (S_{32S}) better than 24 dB.

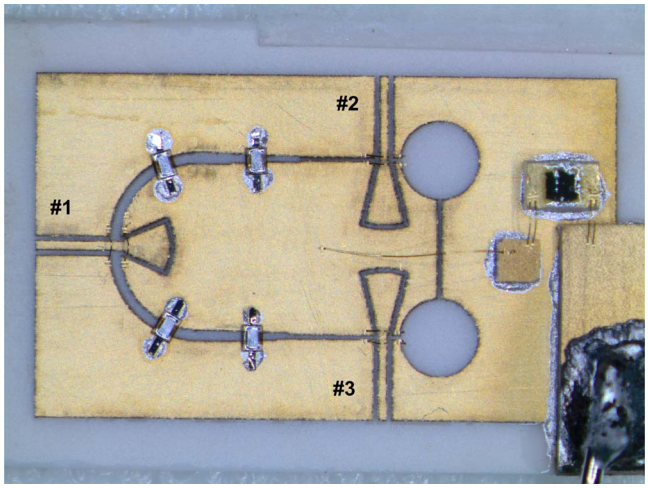

FIG. 12. Photograph of the CPW-slotline SPDT with four PIN diodes as switching devices and the bias network.

The bias network of the diodes is implemented by a quarter-wavelength bonding wire (diameter d = 25 μm), a capacitor C = 0.5 pF, and a series resistor R = 10 Ω. The results are performed for a 20 mA forward current per diode and state, so the total DC current consumption is 40 mA/state. The performance improves the bandwidth and return loss using hybrid technology with discrete PIN diodes compared with a Ka-band waveguide approach.[24]

C. SPDT-BPF-SPDT interaction analysis

In this section, the analysis described in Sec. II C is performed with measured S-parameters of the SPDT and BPFs. The errors introduced in terms of phase difference and

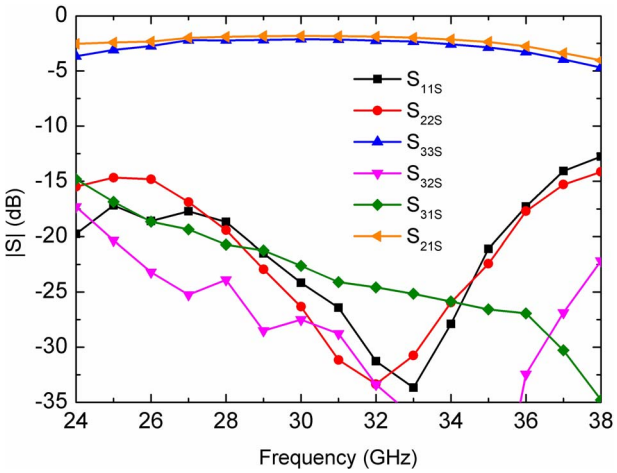

FIG. 13. SPDT measured S-parameters using four PIN diodes.

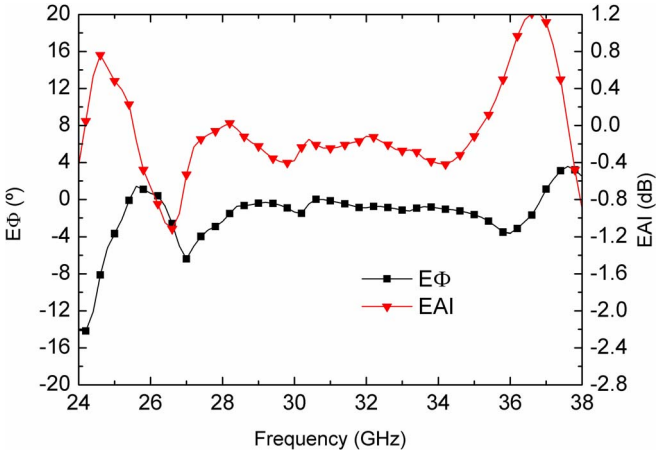

FIG. 14. Errors in phase ($E\Phi$) and amplitude imbalance (EAI) of the phase switch relative to measured BPFs.

amplitude imbalance relative to the measurements of the BPFs are shown in Fig. 14. Phase and amplitude imbalance errors better than 6.4° and 1.1 dB are expected for the integrated phase switch.

D. Phase switch characterization

To validate the complete phase switch design, the BPFs and the SPDT are integrated in planar technology. The phase switch circuit is shown in Fig. 15, in which top and bottom views are depicted. The bottom view shows the absence of metallization in the backside of the SPDTs over its CPW and slotline parts, while for its microstrip line and the BPFs the back metallization is provided.

The whole circuit is implemented and tested in a coplanar probe station. The phase switch is characterized with PIN diodes and the performance for a total DC current consumption of 80 mA is shown in Fig. 16. The measurements for each phase switch state show return loss better than 11 dB and insertion loss of around 4 dB over the frequency band from 26 to 36 GHz, with an average phase difference of $87.1° \pm 4°$ and an average amplitude imbalance of 0.3 dB. The reduction in the working bandwidth from the BPF characterization is due to mismatching effects between SPDT and BPFs and, also, imperfections in fabrication of the full circuit. As a conclusion, the integration of the SPDT circuit in the phase switch has demonstrated an excellent performance with low *PE* and *AI*.

A comparison with other previously reported works is shown in Table II. The lack of broadband integrated phase switch circuits at these frequencies makes difficult the comparison. The results obtained are outstanding compared to other phase shifters taking into account the complexity due to the frequency range, since relative bandwidths greater than

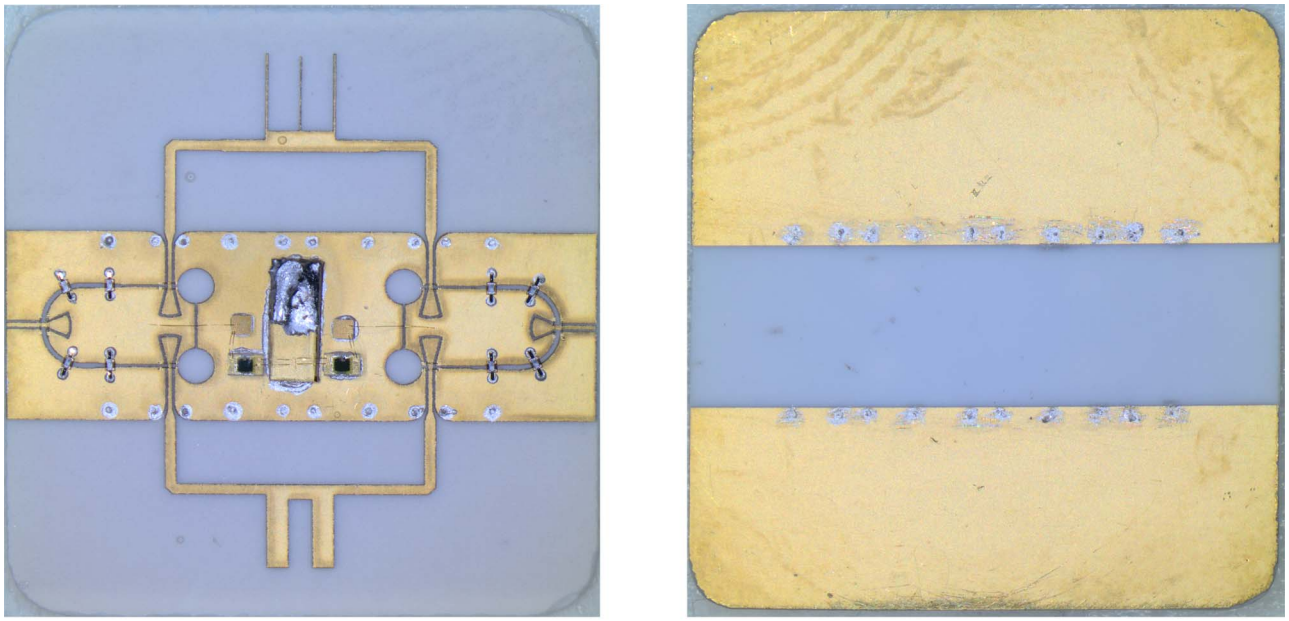

(a) (b)

FIG. 15. Photograph of the full integrated phase switch circuit. (a) Top view. (b) Bottom view.

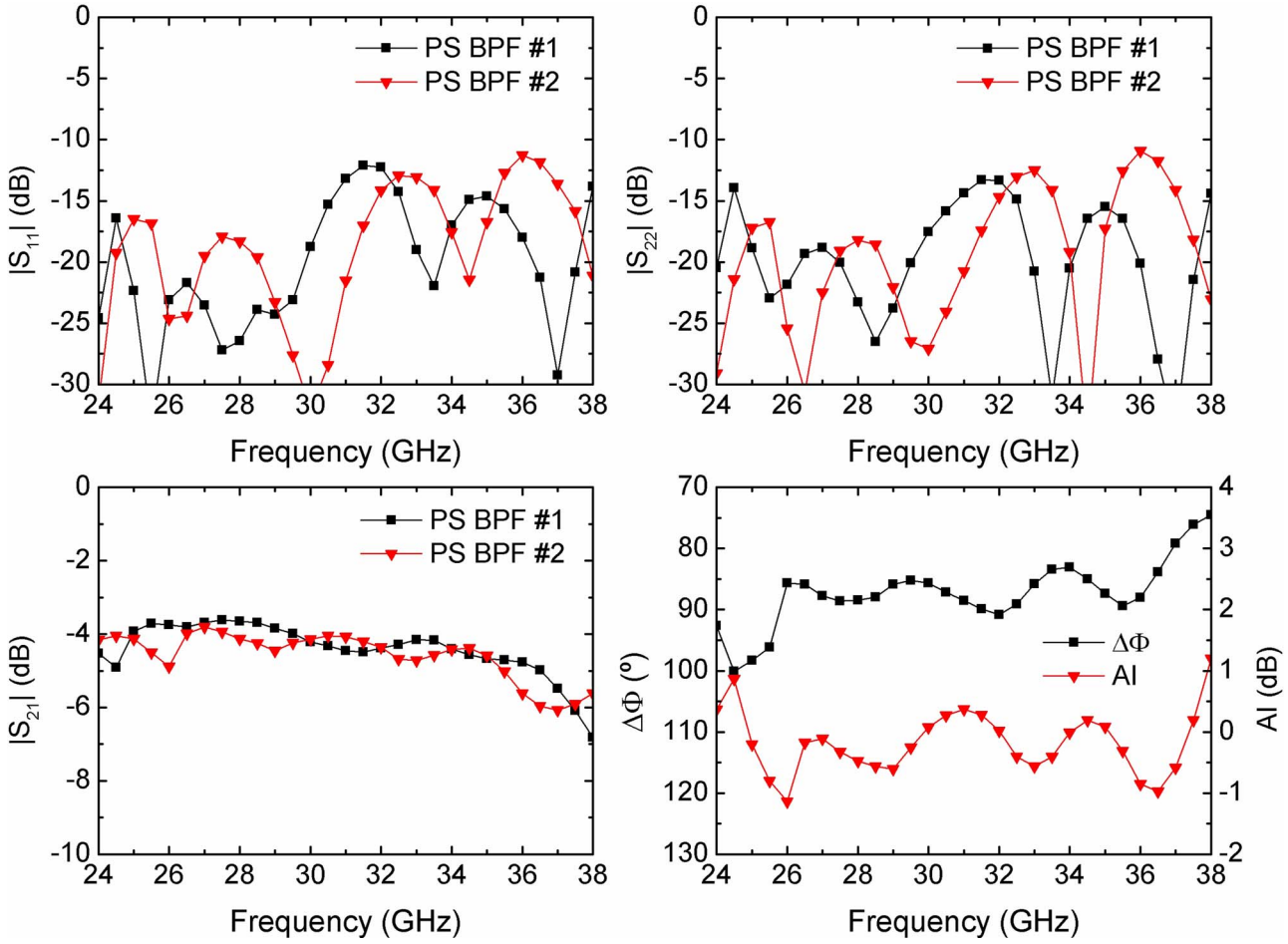

FIG. 16. Phase switch circuit measurements: S-parameters for both transmission branches, phase difference ($\Delta\Phi$), and amplitude imbalance (*AI*).

30% are difficult to obtain. Besides, the integration of the full circuit shows better reliability, *PE* and *AI* in the band of interest with lower insertion loss than design reported by Villa *et al.*,[17] in which bonding wire interconnections between subsystems are critical because of their direct impact in phase results. These facts ensure also a higher repeatability for a multipixel receiver.[22,23]

TABLE II. Comparison of wideband 90° phase switches.

Type	Frequency (GHz)	Relative BW (%)	PE (°)	AI (dB)	IL (dB)	RL (dB)
Loaded line[2]	2.3–5.5	82	6.4[a]	...	0.6	10
Coupled lines[4]	3–7	80	4[a]	...	<2.5	13
Transmission lines[6]	3–11	114	3[a]	...	<0.4	15
Schiffman type[7]	1.5–3.1	69	5[a]	...	0.5	12
BPF-line[10]	1–2	66	2.1	...	<0.5	18
BPF-line[12]	1–3	100	2.5[a]	...	<0.5	12
Transmission lines[15]	2.02–6.18	101	5[a]	...	<1.2	12
Reflection-type[16]	0.8–2.6	105	1.9	0.34	<2.8	10
BPF-BPF[17]	24–37	42	6	0.5	4.5	15
Transmission lines[21]	40	...	3.3	0.008	4.4	20
This work	24–37	42	5[a]	0.15	0.5	13
	26–36	33	1.1[a]	0.15	0.5	13
This work	26–36	33	4	0.3	4	11

[a]Switch function not integrated.

V. CONCLUSION

The analysis, design, and characterization of a 90° phase switch working in the Ka-band are described. The proposed configuration uses broadband SPDTs on planar technology integrated with wideband phase shifting branches based on BPF designs. The full analysis of π-network BPFs is performed in order to obtain the phase difference by sweeping the optimum impedance ratio for quarter- and half-wavelength electrical lengths taking into account the minimum phase error and amplitude imbalance. The relationships between the two BPFs in terms of phase difference, relative phase error, and amplitude imbalance are established. Individual BPFs are designed and tested, with return loss better than 13 dB and insertion loss of about 0.5 dB; the phase difference shows an average value of 88.9° ± 5° and an average amplitude imbalance of 0.15 dB from 24 to 37 GHz (relative bandwidth of 42 %). A novel broadband SPDT switch using PIN diodes as switching devices is designed and tested, showing isolation better than 19 dB with insertion loss of about 1.8 dB and return loss better than 15 dB. The full integration of the phase switch provides return loss better than 11 dB and insertion loss of around 4 dB over the frequency band from 26 to 36 GHz; an average phase difference of 87.1° ± 4° and average amplitude imbalance of 0.3 dB is obtained. The results obtained are outstanding taking into account the complexity due to the frequency range and to the effects that the SPDT

adds to the performance regarding the individual branches. Moreover, the phase switch designed is suitable for radio-astronomy receivers based on differential schemes with phase switches.

ACKNOWLEDGMENTS

The authors would like to thank the Spanish Ministry for Science and Innovation for the financial support provided under the Project No. AYA2010–21766-C03–03 and the CONSOLIDER-INGENIO 2010 programme under Reference No. CSD2010–00064. The authors also thank Ana Pérez and Eva Cuerno, both with the Department of Communications Engineering, for their assistance in circuit manufacture and assembly.

[1]B. M. Schiffman, IRE Trans. Microwave Theory Tech. **6**, 232 (1958).
[2]S. Zheng, W. Chan, and K. Man, IEEE Microw. Wirel. Compon. Lett. **20**, 498 (2010).
[3]X. Tang and K. Mouthan, "Dual-band class III loaded-line phase shifters," in *Asia-Pacific Microwave Conference Proceeedings*, Yokohama, Japan, 7–10 December 2010, p. 1731–1734.
[4]M. Sorn, R. Lech, and J. Mazur, IEEE Trans. Microwave Theory Tech. **60**, 494 (2012).
[5]Y. Wang, M. E. Bialkowski, and A. M. Abbosh, IEEE Microw. Wirel. Compon. Lett. **22**, 58 (2012).
[6]A. Abbosh, IEEE Microw. Wirel. Compon. Lett. **21**, 22 (2011).
[7]Y. X. Guo, Z. Y. Zhang, and L. C. Ong, Trans. Microwave Theory Tech. **54**, 1196 (2006).
[8]P. Sobis, J. Stake, and A. Emrich, IET Proc. Microwaves, Antennas Propag. **5**, 386 (2011).
[9]S. Y. Eom, IEEE Microw. Wirel. Compon. Lett. **14**, 228 (2004).
[10]X. Tang and K. Mouthan, Trans. Microwave Theory Tech. **58**, 1573 (2010).
[11]X. Tang and K. Mouthan, Trans. Microwave Theory Tech. **58**, 3459 (2010).
[12]X. Tang and K. Mouthan, IEEE Microw. Wirel. Compon. Lett. **19**, 506 (2009).
[13]S. Y. Eom and H. K. Park, Microwave Opt. Technol. Lett. **38**, 255 (2003).
[14]G. J. Sung, "Broadband 90° phase shifter using two short stubs," in *Proceedings of the IEEE Radio and Wireless Symposium*, *New Orleans, Louisiana*, 10–14 January 2010, pp. 464–467.
[15]S. H. Yeung, Q. Xue, and K. F. Man, IEEE Trans. Microwave Theory Tech. **60**, 2760 (2012).
[16]H. R. Fang, X. Tang, K. Mouthaan, and R. Guinvarc'h, IEEE Trans. Microwave Theory Tech. **60**, 3440 (2012).
[17]E. Villa, L. de la Fuente, J. Cagigas, B. Aja, and E. Artal, Electron. Lett. **49**, 349 (2013).
[18]B. Aja, E. Artal, L. de la Fuente, J. P. Pascual, A. Mediavilla, N. Roddis, D. Kettle, W. F. Winder, L. Pradell, and P. de Paco, IEEE Trans. Microwave Theory Tech. **53**, 2050 (2005).
[19]P. Kangaslahti, T. Gaier, M. Seiffert, S. Weinreb, D. Harding, D. Dawson, M. Soria, C. Lawrence, B. Hooberman, and A. Miller, "Planar polarimetry receivers for large imaging arrays at Q-band," in *Proceedings of the IEEE MTT-S International Microwave Symposium Digest*, San Francisco, California, 11–16 June 2006, pp. 89–92.
[20]D. Kettle and N. Roddis, IEEE Trans. Microwave Theory Tech. **55**, 2700 (2007).
[21]M. Sieth, J. M. Lau, P. Voll, S. Church, P. Kangaslahti, L. Samoska, M. Soria, T. Gaier, D. van Winkle, J. Neilson, S. Tantawi, K. Cleary, and A. C. S. Readhead, Proc. SPIE **7741**, 77412I (2010).
[22]J. A. Rubiño-Martin, R. Rebolo, M. Tucci, R. Génova-Santos, S. R. Hildebrandt, R. Hoyland, J. M. Herreros, F. Gómez-Renasco, C. López, E. Martínez-González, P. Vielva, D. Herranz, F. J. Casas, E. Artal, B. Aja, L. de la Fuente, J. L. Cano, E. Villa, A. Mediavilla, J. P. Pascual, L. Piccirillo, B. Maffei, G. Pisano, R. A. Watson, R. Davis, R. Davies, R. Battye, R. Saunders, K. Grainge, P. Scott, M. Hobson, A. Lasenby, G. Murga, C. Gómez, A. Gómez, J. Arino, R. Sanquirce, J. Pan, A. Vizcarguenaga, and B. Etxeita, *Highlights of Spanish Astrophysics V, Astrophysics and Space Science Proceedings* (Springer, Berlin, 2010), Part 3, pp. 127–135.
[23]J. L. Cano, E. Villa, J. Cagigas, B. Aja, J. V. Terán, A. R. Pérez, L. de la Fuente, E. Artal, A. Mediavilla, and R. Hoyland, "Multi-pixel Ka-band radiometer for the QUIJOTE experiment (Phase II)," in *Proceedings of the 42nd European Microwave Conference*, Amsterdam, The Netherlands, October 2012, pp. 37–40.
[24]G. A. Kumar and A. Kumar, "Low loss and high isolation Ka-band SPDT switch," in *Proceedings of the 5th International Conference on Computers and Devices for Communication* (2012), p. 1.